Supporting Information for

The Electromagnetic Absorption of a Na-ethylenediamine Graphite Intercalation Compound

Le Quan,[1,2] Hanyang Zhang,[1*] Huijie Wei,[2] Yunqing Li,[1] Sung O Park,[3] Dae Yeon Hwang,[3] Yu Tian,[2] Ming Huang,[1] Chunhui Wang,[1] Meihui Wang,[1] Sang Kyu Kwak,[3] Faxiang Qin,[2]

Hua-Xin Peng,[2] Rodney S. Ruoff[1,4,5,6 *]

1.Center for Multidimensional Carbon Materials (CMCM), Institute for Basic Science (IBS), Ulsan 44919, Republic of Korea

2.Institute for Composites Science Innovation (InCSI), School of Materials Science and Engineering, Zhejiang University, Hangzhou, 310027, China

3.School of Energy and Chemical Engineering, Ulsan National Institute of Science and Technology (UNIST), Ulsan 44919, Republic of Korea

4. School of Materials Science and Engineering, UNIST, Ulsan 44919, Republic of Korea.

5. Department of Chemistry, UNIST, Ulsan 44919, Republic of Korea.

6. School of Energy and Chemical Engineering, UNIST, Ulsan 44919, Republic of Korea

Correspondence

Hanyang Zhang, zhanghanyang5@gmail.com

Rodney S. Ruoff, ruofflab@gmail.com; rsruoff@ibs.re.kr

Section 1

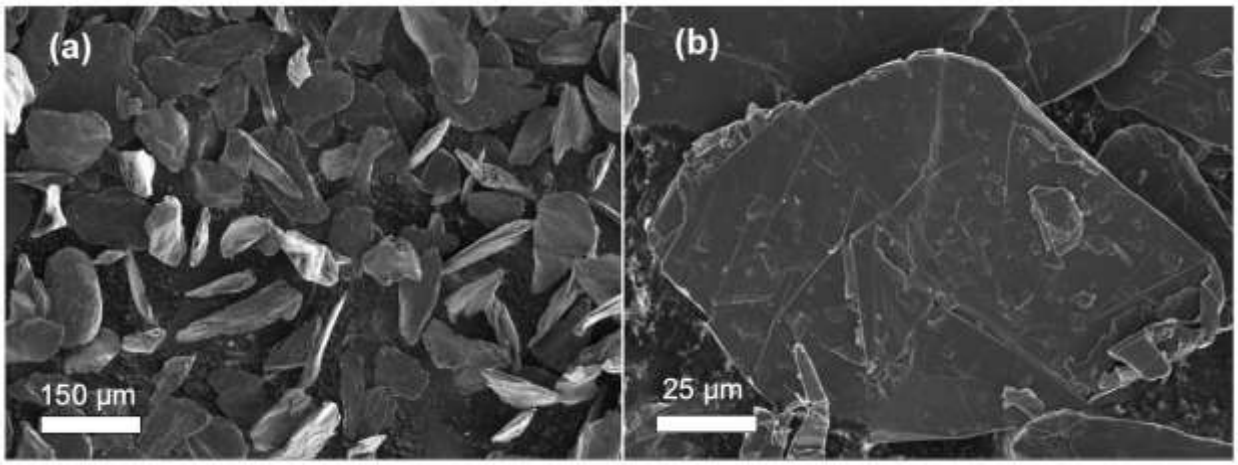

Figure S1. (a) and (b) 5.00 kV SEM images of the morphology of graphite powder.

Section 2

To investigate the origin of the enhanced electrical conductivity of GIC, spin-polarized density functional theory (DFT) calculations were carried out by Cambridge Serial Total Energy Package (CASTEP).[S1] The generalized gradient approximation with Perdew-Burke-Ernzerhof (GGA-PBE) function was used to describe the exchange-correlation potentials in the calculation.[S2] For the van der Waals dispersion corrections, Grimme's method of DFT-D2 scheme was employed. [S3] Norm-conserving pseudopotential was applied to represent the electron-ion interactions under the plane-wave energy cutoff of 700 eV. The Brillouin zone was sampled by the Monkhorst-Pack scheme using the *k*-point separation of 0.03 $Å^{-1}$; the applied *k*-point grids were 15 × 15 × 6 for bulk graphite and 5 × 5 × 5 for GIC, respectively.[S4] After optimizing the structures of Gt and GIC, we calculated their band structures under the *k*-point grids of 60 × 60 × 20 and 20 × 20 ×19, respectively, and compared.

In the band structure of Gt, the bonding π bands and the anti-bonding π^* bands are located near the Fermi level, which exhibits semi-metallic characters (Figure S2d). When Na and ethylenediamine are intercalated, the π^* bands, unoccupied before the intercalation, become partially occupied by the reduction of Gt. Correspondingly, delocalized bands are formed across the Fermi level along the Γ-M-K plane (i.e., in-plane), which contribute to the metallic characters of GIC (Figure S2e). Thus, GIC can have higher electrical conductivity than Gt along the in-plane direction. While in both Gt and GIC, the bands are separated and localized along the Γ-A line, i.e., perpendicular to the basal plane, which induce lower electrical conductivity than that in in-plane direction.

We also measured the conductivity of Na(ethylenediamine)C_{15} made from its parent graphite (Table S1). Gt as well as GIC powder was cold pressed into square thin films

(1.0 cm × 1.0 cm, with a typical thickness of 400 μm) under ~66 MPa pressure. Additionally, we synthesized the same GIC species with a commercial graphite foil from Alfa Aesar and measured the conductivity.

All samples' electrical conductivities were measured and calculated using a Keithley 4200 semiconductor characterization system with probe station.

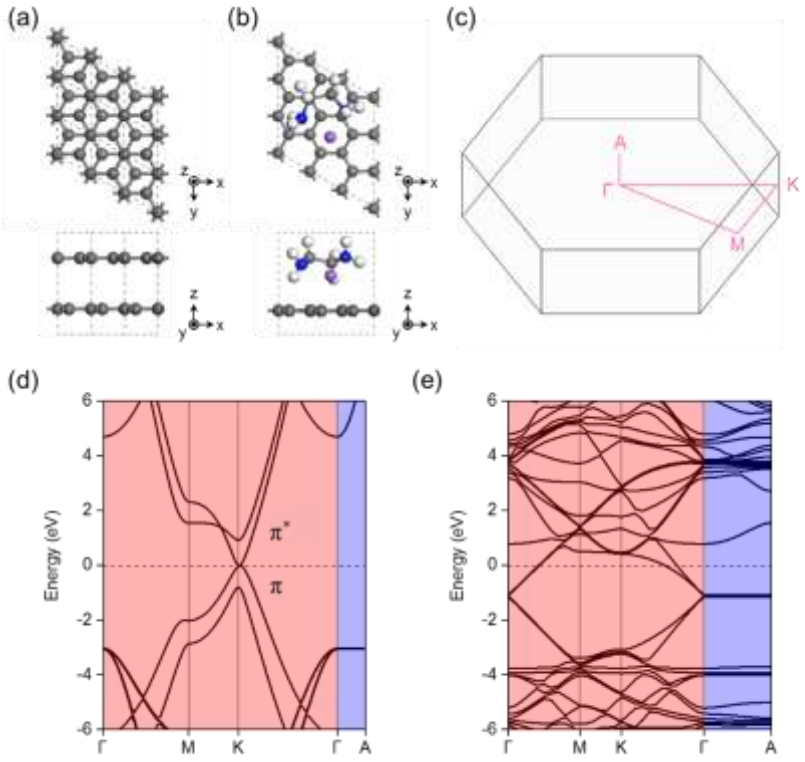

Figure S2. Top and side views of model systems used in DFT calculations: (a) Gt and (b) GIC. The dark gray, white, blue, and purple spheres represent carbon, hydrogen, nitrogen, and sodium atoms, respectively. (c) The Brillouin zone for Gt and GIC. Band structures of (d) bulk graphite and (e) GIC along in-plane (red shaded area) and perpendicular direction to the basal plane (blue shaded area). The Fermi level (E_F) was set to be 0 eV.

Section 3

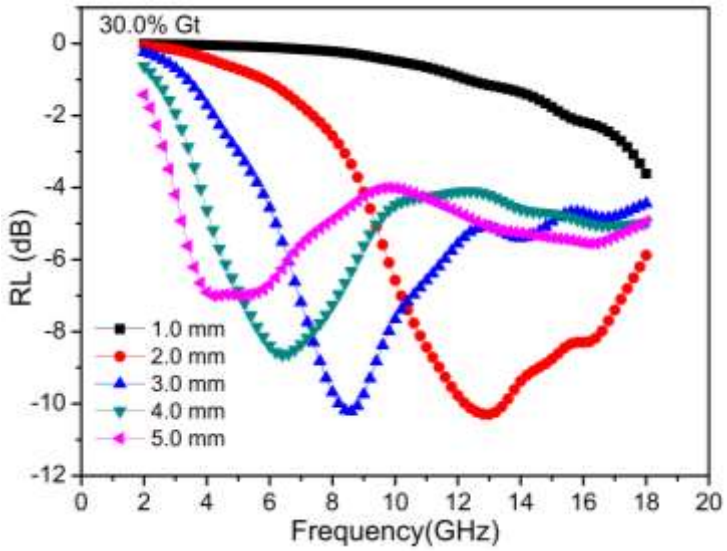

Figure S3. Frequency dependence of the reflection loss of the 30.0 wt% graphite sample with varying thicknesses.

Section 4

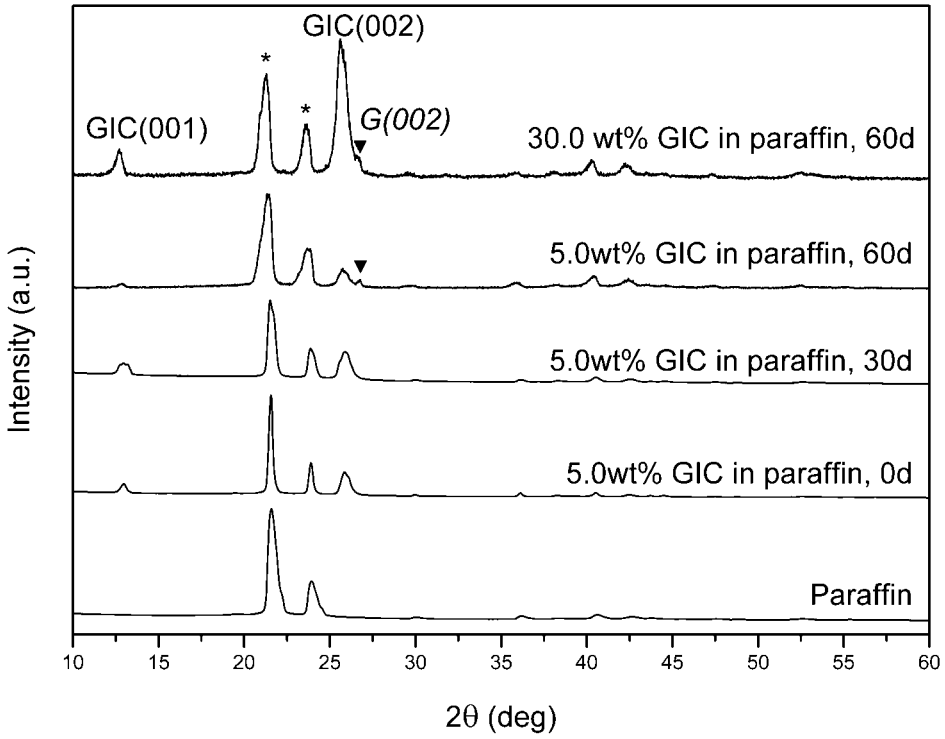

Figure S4. The stability in air of GIC in paraffin at ambient conditions. The PXRD patterns show the 5.0 wt% GIC (featured by GIC 001 and 002 peaks) in paraffin after 0, 30 and 60 days, and 30.0 wt% GIC in paraffin after 60 days. The asterisk (*) indicates the paraffin peaks and the inverted triangle (▼) the (minor) graphitic (002) peak.

Section 5

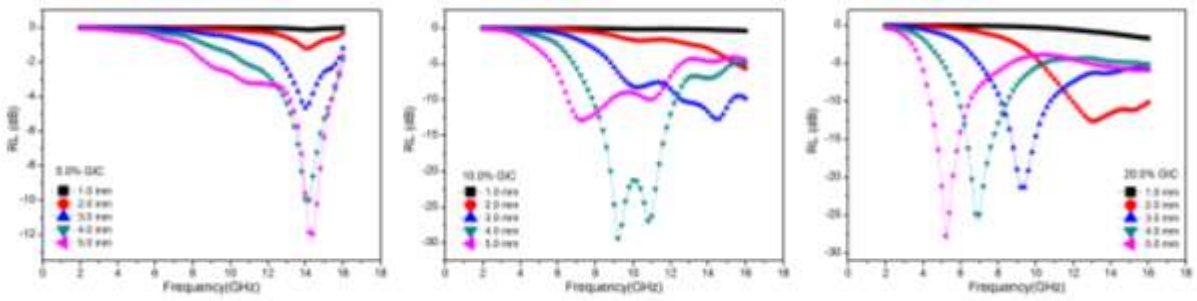

Figure S5. Frequency dependence of the reflection loss of the 5.0, 10.0 and 20.0 wt% GIC samples after 60 days in ambient conditions.

The RL of original optimal 10.0 wt% loaded sample has dropped but is still usable up to -30 dB and comparable with the 20.0 wt% sample after 60 days.

Section 6

Table S1 The absorption performance of graphite/graphene based absorption agents in the laboratory as well as common commercial absorption agents for civil use.

Graphene based composites	**Filler content**	**Performance from filler or composite**	**RL maximum, bandwidth of RL<-10dB (investigated regions), and the thickness**	**Ref.**
rGO			-6.8 dB (2~18 GHz) 2mm	S5
Graphene foam			-34 dB 14.3GHz (2~18GHz), not given	S6
rGO/Ni/paraffin	60 wt%	filler	-17 dB 3.0~4.0 GHz, 12.0~14.0 GHz (2~18 GHz) 5mm	S7
Cobalt/epoxy resin	30 wt%	composite	-45 dB 12~18 GHz (2~18 GHz) 1.5mm	S8
Fe_3O_4/graphene/paraffin	20 wt%	filler	-53.2 dB 9~15GHz (2~18 GHz) 2.5mm	S9
ZnO-coated Fe nanocapsules	40 wt%	filler	-57.1 dB 7~10GHz (2~18 GHz) 3mm	S10
C/Co	15 wt%	filler	-52.3 dB 5.1GHz (2~18 GHz) 2mm	S11
Fe_xO_y/Fe decorated graphite	1:3	filler	-42.1 dB 11.04~15.44 GHz (2~18 GHz) 2mm	S12
ZnO/graphene/paraffin	80 wt%	filler	-52 dB 3.2~17 GHz (2~18 GHz) 1.5mm	S13
rGO/PVA	0.9 wt%	composite	-36.4 dB 3.8~5.4 GHz (2~18GHz) 5mm	S14
rGO/NBR	10 wt%	composite	-57 dB 7.5~12 GHz (4~12 GHz) 3mm	S15
Na(en)C_{15}/paraffin	10 wt%	filler	-75.6 dB 9.25 GHz (8~12GHz) 4.0mm	This work
Commercial absorbers for civil use	**Common filler and matrix**		**Common performance (technical parameters from supplier)**	**Source**
broadband pyramidal absorber	ferrite materials/PU		better than -30 dB 10~35 GHz 30 mm ~ -50~-60 dB 3~40 GHz 1000 mm	S16-17
flexible ferrite sheet	ferrite and metal (Mg, Cu, Fe, Ni, Co etc) particles in resin		very diverse, usually no better than -15 dB 1~18GHz <8 mm	S18
ferrite tile absorber	ferrite		-10dB~-50dB 30MHz~1GHz 4-27 mm	S19
NSSR Series narrowband absorber (Kitagawa inc.)	unknown		better than -35 dB 4.3~18GHz 0.5-4.0 mm	S20

REFERENCES IN SUPPORTING INFORMATION

(S1) Clark, S. J.; Segall, M. D.; Pickard, C. J.; Hasnip, P. J.; Probert, M. J.; Refson, K.; Payne, M. C. First Principles Methods Using CASTEP. *Z. Kristallogr.*, **2005**, *220*, 567-570.

(S2) Perdew, J. P.; Burke, K.; Ernzerhof, M. Generalized Gradient Approximation Made Simple. *Phys. Rev. Lett.*, **1996**, *77*, 3865.

(S3) Grimme, S. Semiempirical GGA-Type Density Functional Constructed with A Long-Range Dispersion Correction. *J. Comput. Chem.*, **2006**, *27*, 1787.

(S4) Monkhorst, H. J.; Pack, J. D. Special Points for Brillouin-Zone Integrations. *Phys. Rev. B* **1976**, *13*, 5188.

(S5) Wang, C.; Han, X.; Xu, P.; Zhang, X.; Du, Y.; Hu, S.; Wang, J.; Wang, X. The Electromagnetic Property of Chemically Reduced Graphene Oxide and Its Application as Microwave Absorbing Material. *Appl. Phys. Lett.,* **2011,** *98*, 072906.

(S6) Zhang, Y.; Huang, Y.; Chen, H.; Huang, Z.; Yang, Y.; Xiao, P.; Zhou, Y.; Chen, Y. Composition and Structure Control of Ultralight Graphene Foam for High-Performance Microwave Absorption. *Carbon* **2016,** *105*, 438-447.

(S7) Chen, T.; Deng, F.; Zhu, J.; Chen, C.; Sun, G.; Ma, S.; Yang, X. Hexagonal and Cubic Ni Nanocrystals Grown on Graphene: Phase-Controlled Synthesis, Characterization and Their Enhanced Microwave Absorption Properties. *J. Mater. Chem.*, **2012,** *22*, 15190-15197.

(S8) He, C.; Qiu, S.; Wang, X.; Liu, J.; Luan, L.; Liu, W.; Itoh, M.; Machida, K.-i. Facile Synthesis of Hollow Porous Cobalt Spheres and Their Enhanced Electromagnetic

Properties. *J. Mater. Chem.*, **2012,** *22*, 22160-22166.

(S9) Zhang, R.; Huang, X.; Zhong, B.; Xia, L.; Wen, G.; Zhou, Y. Enhanced Microwave Absorption Properties of Ferroferric Oxide/Graphene Composites with A Controllable Microstructure. *RSC Adv.* **2016,** *6*, 16952-16962.

(S10) Liu, X. G.; Geng, D. Y.; Meng, H.; Shang, P. J.; Zhang, Z. D. Microwave-Absorption Properties of ZnO-Coated Iron Nanocapsules. *Appl. Phys. Lett.*, **2008,** *92*, 173117.

(S11) Wu, Z.; Pei, K.; Xing, L.; Yu, X.; You, W.; Che, R. Enhanced Microwave Absorption Performance From Magnetic Coupling of Magnetic Nanoparticles Suspended within Hierarchically Tubular Composite. *Adv. Funct. Mater.*, **2019,** *29*, 1901448.

(S12) Meng, R.; Zhang, T.; Yu, H.; Zhang, J.; Wen, G.; Huang, X.; Huang, L.; Xia, L.; Zhong, B. A Facile Coprecipitation Method to Fe_xO_y/Fe Decorated Graphite Sheets with Enhanced Microwave Absorption Properties. *Nanotechnology* **2019,** *30*, 185704.

(S13) Zhang, B.; Lu, C.; Li, H. Improving Microwave Adsorption Property of ZnO Particle by Doping Graphene. *Mater. Lett.*, **2014,** *116*, 16-19.

(S14) Wang, T.; Li, Y.; Geng, S.; Zhou, C.; Jia, X.; Yang, F.; Zhang, L.; Ren, X.; Yang, H. Preparation of Flexible Reduced Graphene Oxide/Poly (Vinyl Alcohol) Film With Superior Microwave Absorption Properties. *RSC Adv.* **2015,** *5*, 88958-88964.

(S15) Singh, V. K.; Shukla, A.; Patra, M. K.; Saini, L.; Jani, R. K.; Vadera, S. R.; Kumar, N. Microwave Absorbing Properties of A Thermally Reduced Graphene Oxide/Nitrile Butadiene Rubber Composite. *Carbon* **2012,** *50*, 2202-2208.

(S16) Web commerial information: https://hollandshielding.com/Wide-band-hybrid-pyramid-EM-absorbers

(S17) Web commerial information: http://www.emcsky.com/en/detail.asp?id=95

(S18) Web commerial information: https://hollandshielding.com/Ferrite-tiles-flexible-absorber-sheets-foam-pyramidal

(S19) Web commerial information: https://www.djmelectronics.com/rf-absorber.html

(S20) Web commerial information: http://kgs-ind.com/products/emc/emi-absorbers/emi-absorber-sheets-narrow-band-type/nssr-series/